Locomotion induced by medial septal glutamatergic neurons is linked to intrinsically generated persistent firing

Karolína Korvasová[1,2,3*], **Felix Ludwig**[4], **Hiroshi Kaneko**[4,5], **Liudmila Sosulina**[4,5], **Tom Tetzlaff**[1], **Stefan Remy**[4,5], **Sanja Mikulovic**[4,6,*]

***For correspondence:**
karolina.korvasova@mff.cuni.cz (Karolína Korvasová); sanja.mikulovic@lin-magdeburg.de (Sanja Mikulovic)

[1]Institute of Neuroscience and Medicine (INM-6) and Institute for Advanced Simulation (IAS-6) and JARA-Institute Brain Structure-Function Relationships (INM-10), Jülich Research Centre, Jülich, Germany; [2]RWTH Aachen University, Aachen, Germany; [3]Faculty of Mathematics and Physics, Charles University, Prague, The Czech Republic; [4]Neuronal Networks Group, German Center for Neurodegenerative Diseases, Bonn, Germany; [5]Department of Cellular Neuroscience, Leibniz Institute for Neurobiology, Magdeburg, Germany; [6]Cognition and Emotion Laboratory, Leibniz Institute for Neurobiology, Magdeburg, Germany

Abstract

Medial septal glutamatergic neurons are active during theta oscillations and locomotor activity. Prolonged optogenetic activation of medial septal glutamatergic neurons drives theta oscillations and locomotion for extended periods of time outlasting the stimulus duration. However, the cellular and circuit mechanisms supporting the maintenance of both theta oscillations and locomotion remain elusive. Specifically, it remains unclear whether the presence of theta oscillations is a necessary prerequisite for locomotion, and whether neuronal activity within the medial septum underlies its persistence. Here we show that a persistent theta oscillation can be induced by a brief transient activation of glutamatergic neurons. Moreover, persistent locomotion is initiated even if the theta oscillation is abolished by blocking synaptic transmission in the medial septum. We observe persistent spiking of medial septal neurons that outlasts the stimulus for several seconds, both in vivo and in vitro. This persistent activity is driven by intrinsic excitability of glutamatergic neurons.

Introduction

The medial septum and diagonal band of Broca (MSDB) is the main generator of hippocampal theta oscillations (***Buzsáki, 2002***) and septo-hippocampal projections control hippocampal neuronal excitability during locomotion and other types of behavior (***Fuhrmann et al., 2015***; ***Müller and Remy, 2018***). While a significant amount of research addressed the role of GABAergic and cholinergic MSDB neurons and their septo-hippocampal projections (***Brashear et al., 1986***; ***Markram and Segal, 1990***; ***Toth et al., 1993***; ***Müller and Remy, 2018***), the important role of glutamatergic MSDB neurons has emerged only recently (***Manseau et al., 2005***; ***Huh et al., 2010***; ***Leao et al., 2015***; ***Robinson et al., 2016***; ***Fuhrmann et al., 2015***; ***Zhang et al., 2018***; ***Dannenberg et al., 2019***). We

previously demonstrated that MSDB glutamatergic neurons, which predominantly expressed the vesicular glutamate transporter 2 (VGluT2), increased their activity several hundred milliseconds before the onset of locomotion and that their physiological in vivo activity positively correlated with the velocity of locomotion (***Fuhrmann et al., 2015***). Stimulating these VGluT2 neurons in the theta frequency range induced combined theta activity in the hippocampus and locomotion, which both persisted for several seconds after the stimulus offset (***Fuhrmann et al., 2015***; ***Justus et al., 2017***). The continuous stimulation of VGluT2 MSDB neurons at different frequencies evoked hippocampal theta oscillations which were locked to the stimulation frequency. In addition, both the induced hippocampal oscillation as well as the induced locomotion seized with stimulation-offset (***Fuhrmann et al., 2015***). Since in these experiments the firing of VGluT2 neurons and the resulting theta oscillation were entrained by the optogenetic stimulation, the mechanisms governing the prolonged elevated activity of MSDB glutamatergic neurons during physiological theta oscillations and more naturally initiated locomotion remain unknown. Moreover, it is unknown whether the ongoing activity of VGluT2 is causally underlying the persistence of theta activity and locomotion after the stimulus offset.

Persistent firing, a sustained change in neural activity discharge that outlasts the stimulus offset, has been most frequently referred to represent the neural correlate underlying working memory (***Fuster, 1973***; ***Kubota et al., 1974***; ***Zylberberg and Strowbridge, 2017***). It was traditionally linked to the cortical regions where it was shown to depend on the cholinergic activation and network mechanisms (***Jochems and Yoshida, 2013***; ***Zylberberg and Strowbridge, 2017***). Up till now, persistent firing was reported in multiple primates' cortical areas including auditory cortex (***Gottlieb et al., 1989***), visual cortex (***Supèr et al., 2001***) and somatosensory cortex (***Zhou and Fuster, 1996***), as well as in the cortical regions in humans (***Todd and Marois, 2004***; ***Schluppeck et al., 2006***; ***Srimal and Curtis, 2008***). Increasing body of evidence (***Pastalkova et al., 2008***; ***Yoshida and Hasselmo, 2009***; ***MacDonald et al., 2011***; ***Harvey et al., 2012***) convincingly shows the existence of persistent firing in rodents too, in both cortical and subcortical structures (***Egorov et al., 2006***; ***Tian et al., 2014***; ***O'Malley et al., 2020***; ***Zylberberg and Strowbridge, 2017***). Recent results supported a more general behavioral importance of persistent firing beyond the working memory, including reinforcement learning, decision making and innate defensive behaviour (***Seo et al., 2007***; ***Barraclough et al., 2004***; ***Seo et al., 2009***; ***Histed et al., 2009***; ***Kennedy et al., 2020***) and motor control (***Kiehn and Eken, 1998***). While the importance of MSDB circuits and theta oscillations was linked to several of these behaviours (***Turnbull et al., 1994***; ***McNaughton et al., 2006***; ***Shirvalkar et al., 2010***; ***Lipponen et al., 2012***; ***Fuhrmann et al., 2015***), no study previously demonstrated the existence of persistent activity in the MSDB.

Here, we report that hippocampal theta activity and locomotion can be reliably triggered by a brief non-periodic stimulation of MSDB VGluT2 neurons. Further, we demonstrate that hippocampal theta activity is not necessary for the onset of locomotion. Finally, we show robust persistent firing in the MSDB following transient MSDB-VGluT2 neuron stimulation, both in vivo and in vitro. The persistent firing was also maintained during the synaptic blockade in the MSDB. These results suggest that the stimulus evoked persistent activity is a consequence of the intrinsic single-neuron dynamics in the MSDB VGluT2 neurons.

Results

Brief continuous light stimulation of MSDB VGluT2 neurons initiates locomotion, hippocampal theta and persistent activity in the medial septum

To understand the relation between the local activity of MSDB neurons, CA1 theta oscillations and locomotion, we performed in vivo experiments with head-fixed mice running on a (spherical or linear) treadmill (Figure 1A). We simultaneously monitored locomotion speed, CA1 LFP and MSDB multi-unit activity (Figure 1B). One-second pulses of continuous optical stimulation of MSDB VGluT2 neurons (Figure 1C) reliably induced elevated firing of MSDB neurons, locomotion and CA1 theta

activity in the range $7 - 12$ Hz (Figure 1D, E, Figure S1). Elevated firing of MSDB neurons, CA1 theta activity and locomotion persisted for several seconds after the stimulus offset. Locomotion was typically triggered before the onset of theta activity (Figure 1E upper two panels) and lasted for less than 5 seconds on average (mean 4.4 s, standard deviation 2.9 s). The MSDB persistent spiking went on for at least 20 seconds, when the recording was stopped. Significant increases of CA1 theta power and MSDB firing rate were also observed during the periods of voluntary running (Figure 1F), confirming physiological relevance of the stimulus-induced persistent activity.

To examine whether the intraseptal synaptic connectivity was necessary for the induction of locomotion by MSDB VGluT2 stimulation, we repeated the experiment following the application of a synaptic blocker cocktail (Figure 2A) disrupting glutamatergic, GABAergic and cholinergic synaptic transmission in the MSDB (Figure 2B). A disruption of locomotor induction would indicate that the activation of intraseptal non-glutamatergic neurons would be a necessary condition. Similarly, a blockade of hippocampal theta oscillations would demonstrate a necessary involvement of non-glutamatergic intraseptal circuits. We found a reliable locomotion induction (Figure 2C-E upper panel) and elevated activity of MSDB units during and after the stimulus (Figure 2C-E lower panel, Figure S2), but CA1 theta power significantly decreased (Figure 2C-E middle panel). Hence, the MSDB local network, as well we the CA1 theta oscillation are not necessary for the induction of persistent locomotion. The duration of locomotion was similar as with the intact MSDB network (mean 3.7 s, standard deviation 2.9 s) and the persistent firing lasted until the end of the recording, 20 seconds after the stimulus offset. We observed qualitatively the same results when the mice were running on a spherical or linear treadmill (Figure S3). MSDB persistent activity and locomotion were also reliably initiated and maintained with blocked MSDB glutamatergic synapses only (Figure S4).

MSDB persistent activity is driven by VGluT2 intrinsic mechanisms

To address whether persistent firing is generated intrinsically within the MSDB or driven by the external inputs from other brain areas, we replicated the experiment in a MSDB acute slice preparation (Figure 3A), while recording MSDB extracellular potential using a 6×10 microelectrode array (MEA) (Figure 3B). The slice preparations also pose optimal conditions for mechanistic pharmacological investigation of the cellular mechanisms of persistent firing.

Indeed, during the 1s continuous light stimulus (Figure 3C), MSDB neurons increased their firing rate that stayed elevated for several seconds after the stimulus offset (Figure 3D). Such persistent activity (significantly increased firing rate in the interval $(2, 4)$ seconds, as compared to the baseline calculated from 2 seconds prior to the stimulus onset) was observed in about 20% of cells (Figure 3E). The median firing rate of these cells increased from 5 spikes per second before the stimulus to 12 spikes per second after the stimulus (Figure 3F) and stayed elevated for at least 20 seconds (Figure 3G). The coefficient of variation of the inter-spike intervals showed on average an increase after the stimulus, indicating less regular spiking during post-stimulus persistent activity compared to pre-stimulus spontaneous activity (Figure 3H). It is likely that this effect was caused by recurrent activation of irregularly spiking neurons that did not participate in generation of the theta rhythm. Approximately 20% of cells responded to all stimulus repetitions (Figure 3I).

To test whether the stimulus-induced persistent activity was generated by the intrinsic neuronal dynamics, we applied a synaptic blocker cocktail (Figure 4A) that blocked glutamatergic, GABAergic and cholinergic transmission (Figure 4B). The firing rate increase was still clearly present (Figure 4C) with similar percentage of cells showing persistent activity ($\sim 30\%$). The increase in firing rate was lower (median 6 spikes per second before the stimulus and 9 spikes per seconds after the stimulus) compared to the intact network, where non-stimulated units may have also exhibited increased firing rate after the stimulus due to fast recurrent excitation by VGluT2 neurons. The duration of the trial-averaged response was not affected by the synaptic blocker (Figure 4F). The deregularizing effect visible of the stimulus on unit activity was present but less prominent than under the application of synaptic blockers (Figure 4G). The response reliability was also lower, with

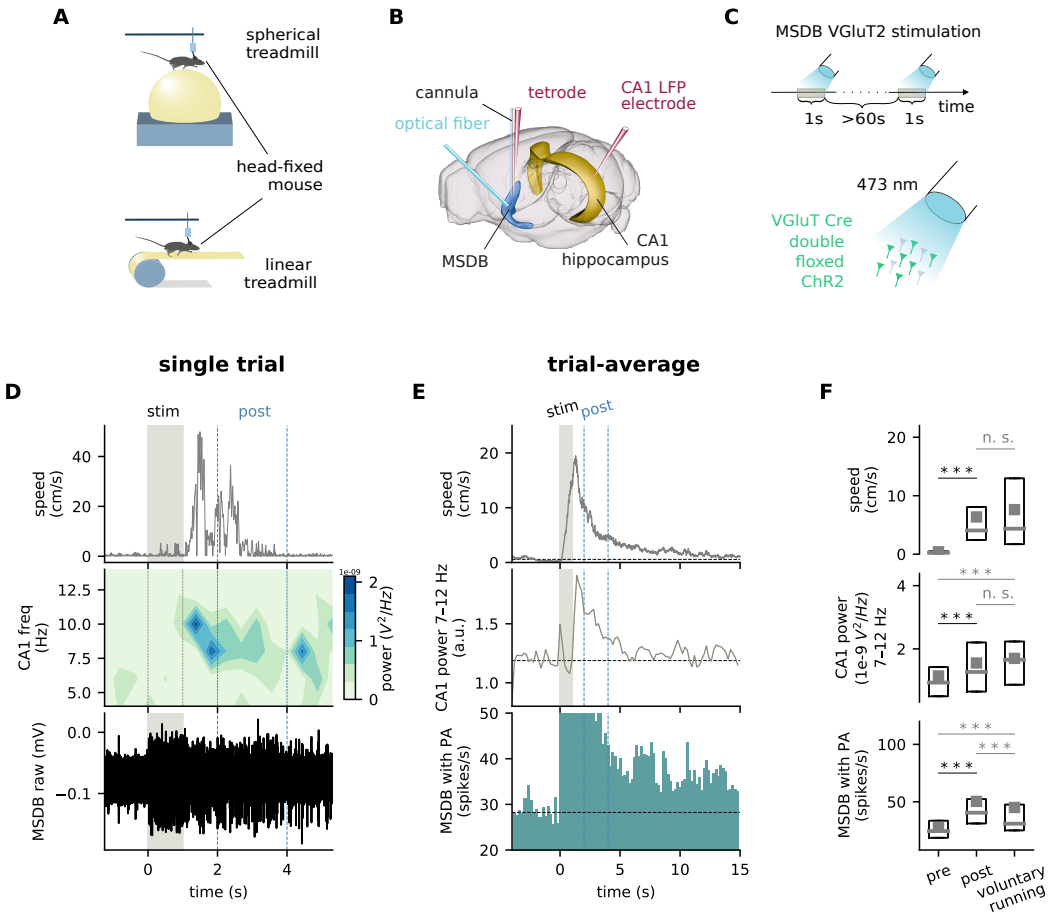

Figure 1. Brief continuous MSDB VGluT2 stimulation triggers persistent activity in the MSDB, locomotion and hippocampal theta.

A. Experimental setup: a head-fixed mouse running on a spherical or linear treadmill. Produced using the SciDraw database (***Branco and Costa, 2020***). **B.** LFP electrode in CA1, optical fiber and tetrode in the MSDB. Produced using The Scalable Brain Atlas (***Bezgin et al., 2009***), based on The Allen Reference Atlas (***Lein et al., 2007***). **C.** Continuous 1s light stimulation of MSDB VGluT2 neurons. **D.** Representative recordings of speed, CA1 LFP with the corresponding spectrogram and MSDB extracellular potential. The grey vertical band marks the continuous light stimulus (0–1 s), the dotted lines mark the time interval used to analyze post-stimulus activity (2–4 s). **E.** Trial-averaged speed (upper panel), CA1 LFP power in the frequency range 7–12 Hz (middle panel) and the average histogram of multi-unit spiking activity of channels with persistent activity (PA) (lower panel). Average across all recording sessions with 4 mice. For significance of a single-channel positive response to one stimulus repetition, $p < 0.05$ from the one-sided Mann-Whitney U-test applied on inter-spike intervals was required. **F.** Distribution of time-averaged speed (upper panel), CA1 LFP power in the range 7–12 Hz (middle panel) and mean firing rate of channels with persistent activity (lower panel) for time periods 2 seconds before the stimulus when the mouse was at rest, in the interval 2–4 seconds and during voluntary running. The bar denotes the median, the square the mean and the box spans between the first and the third quartile. All recordings of 4 mice were used, for firing rates only one channel per mouse was considered. Numbers of trials: 165 trials with one stimulus realization, out of them 122 show persistent activity, 121 trials with voluntary running, out of them 80 show persistent activity. Statistical significance: pre- vs post-stimulus speed $p = 2.6 \cdot 10^{-28}$, post-stimulus vs voluntary running $p = 0.94$, LFP power pre vs post $3 \cdot 10^{-6}$, post-stimulus vs voluntary running $p = 0.07$, pre-stimulus vs voluntary running $p = 1.4 \cdot 10^{-7}$, PA pre vs post $p = 9 \cdot 10^{-22}$, post-stimulus vs voluntary running $p = 0.0007$, pre-stimulus vs voluntary running $p = 7. \cdot 10^{-6}$. The difference between the speed before the stimulus and during voluntary running was significant by construction. Statistical significance was calculated using the two-sided Wilcoxon's signed-rank test for pre- vs post-stimulus difference (black) and the two-sided Mann-Whitney U-test in other cases (grey).

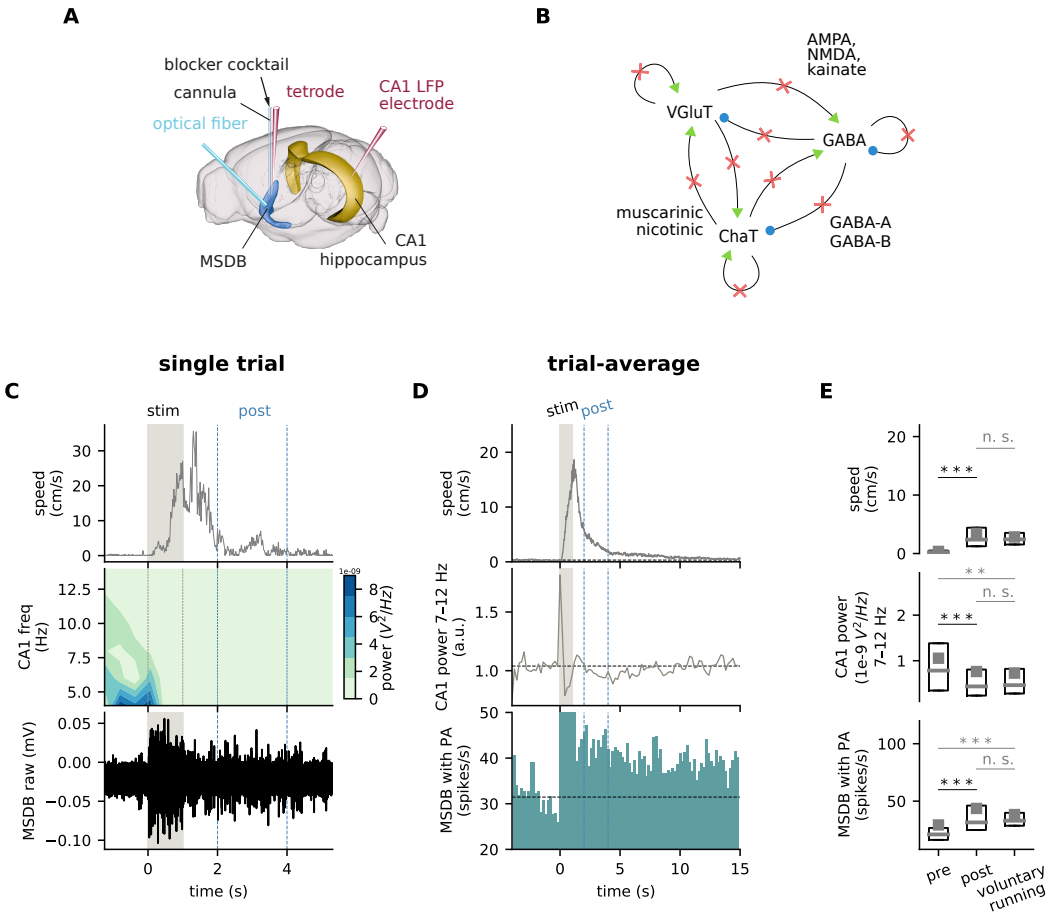

Figure 2. Blocking intraseptal synaptic connectivity abolished CA1 theta, but not locomotion and MSDB persistent activity.

A. Blocker cocktail was applied through a cannula in the MSDB. Produced using The Scalable Brain Atlas (***Bezgin et al., 2009***), based on The Allen Reference Atlas (***Lein et al., 2007***). **B.** Types of synapses blocked by the blocker cocktail. Excitatory synapses are marked by green arrows and inhibitory by blue circles. **C.** Representative recordings of speed, CA1 LFP with the corresponding spectrogram and MSDB extracellular potential. The grey vertical band marks the continuous light stimulus (0–1 s), the dotted lines mark the time interval used to analyze post-stimulus activity (2–4 s). Same mouse as in Figure 1D. **D.** Trial-averaged speed (upper panel), CA1 LFP power in the frequency range 7–12 Hz (middle panel) and the average histogram of multi-unit spiking activity of channels with persistent activity (PA) (lower panel). Average across all recording sessions with 4 mice. For significance of a single-channel positive response to one stimulus repetition, $p < 0.05$ from the one-sided Mann-Whitney U-test applied on inter-spike intervals was required. **E.** Distribution of time-averaged speed (upper panel), CA1 LFP power in the range 7–12 Hz (middle panel) and mean firing rate of channels with persistent activity (lower panel) for time periods 2 seconds before the stimulus when the mouse was at rest, in the interval 2–4 seconds and during voluntary running. The bar denotes the median, the square the mean and the box spans between the first and the third quartile. All recordings of 3 mice were used, for firing rates only one channel per mouse was considered. Numbers of trials intact: 143 trials with one stimulus realization, out of them 76 show persistent activity, 81 trials with voluntary running, out of them 43 show persistent activity. Statistical significance: pre- vs post-stimulus speed $p = 9.6 \cdot 10^{-24}$, post-stimulus vs voluntary running $p = 0.89$, LFP power pre vs post $7.3 \cdot 10^{-6}$, post-stimulus vs voluntary running $p = 0.56$, pre-stimulus vs voluntary running $p = 0.002$, PA pre vs post $p = 3.6 \cdot 10^{-14}$, post-stimulus vs voluntary running $p = 0.52$, pre-stimulus vs voluntary running $p = 5.9 \cdot 10^{-7}$. The difference between the speed before the stimulus and during voluntary running was significant by construction. Statistical significance was calculated using the two-sided Wilcoxon's signed-rank test for pre- vs post-stimulus difference (black) and the two-sided Mann-Whitney U-test in other cases (grey).

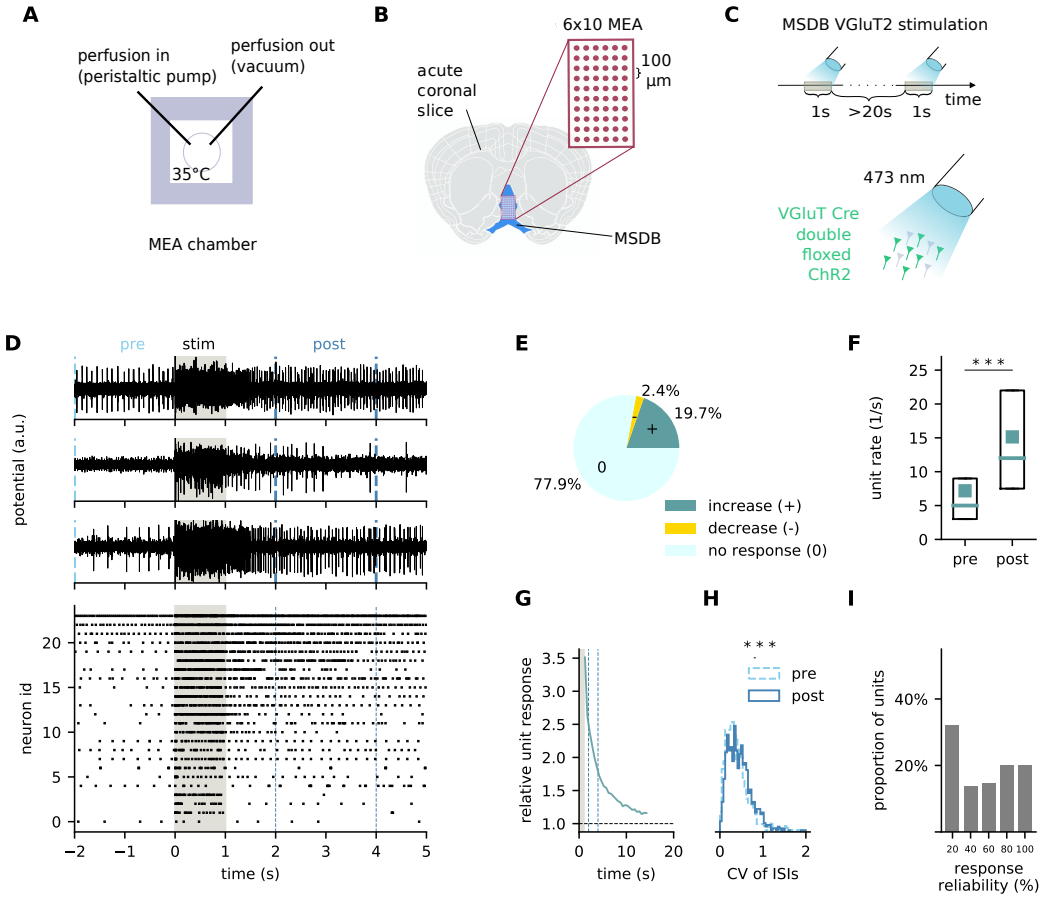

Figure 3. Stimulus-induced persistent activity is generated locally in the MS.
A. Experimental setup: oxygenation chamber. **B.** An acute coronal slice was positioned on a 6x10 MEA with electrode distance $100\ \mu$m. Produced using The Scalable Brain Atlas (***Bezgin et al., 2009***), based on the Allen Reference Atlas (***Lein et al., 2007***). **C.** Continuous 1s light stimulation of MSDB VGluT2 neurons. **D.** Representative traces of the extracellular potential in the acute MSDB slice preparation. The grey vertical bands mark the continuous light stimulus (upper panel). Extracted single-unit activity for one representative slice (lower panel). **E.** Percentages of units with significant increase (dark green), significant decrease (yellow) and no significant change (light green) of firing rate in response to the stimulus. For significance of a single-unit response to one stimulus repetition, $p < 0.05$ from the one-sided Mann-Whitney U-test applied on pre- and post-stimulus inter-spike intervals was required (pre: $(-2, 0)$ s, post: $(2, 4)$ s). **F.** Distribution of firing rates before and after the stimulus (pre: $(-2, 0)$ s, post: $(2, 4)$ s). Only units with persistent activity were considered. Statistical significance of the difference between pooled mean firing rates pre and post: $p = 1.9 \cdot 10^{-40}$ (237 trials, first stimulus). **G.** Trial-averaged time course of single-unit spiking activity. Single stimulus response per unit. **H.** Distribution of coefficients of variation (CV) or inter-spike intervals (ISIs), pre stimulus ($(-2, 0)$ s, blue) and post stimulus ($(2, 4)$ s, red). Single stimulus response per unit. **I.** Percentages of units that respond with given reliability across five stimulus repetitions. Statistical significance was calculated using the two-sided Wilcoxon's signed-rank test. 19 brain slices were used.

up to 55% of units responding to only one stimulus repetition out of five (Figure 4H).

In vivo, the stimulus had a stronger effect when synapses were blocked compared to the intact network (Figure 5A), while the persistent activity did not significantly differ, both in intensity (Figure 5A) and duration (Figure 5B). Differently, the percentage of channels showing persistent activity was larger in the intact than in the blocked network, indicating recruitment of different cell types than VGluT2 to persistent activity by recurrent glutamatergic excitation. Channels showing a significant decrease in firing rate were more frequent in the blocked condition. In both conditions, the highest firing rates after the stimulus occured in channels with high activity during the stimulus, pointing at the involvement of VGluT2 neurons in the persistent activity (Figure 5D).

In the acute MSDB slice preparation, we observed a stronger spiking response in the intact network compared to the blocked condition, both during and after the stimulus (Figure 5E). The duration of persistent activity was comparable in both conditions (Figure 5F), similarly as in vivo. In the acute MSDB slice preparation we also observed a larger proportion of channels with persistent activity in the intact network and a larger proportion of channels with persistent decrease in firing rate in the blocked network (Figure 5G). The positive correlation between the mean firing rate during the stimulus and during the persistent activity in the slice with blocked synapses (Figure 5H, Figure S6B) indicates that the persistent activity is indeed predominantly generated by the VGluT2 intrinsic dynamics.

Discussion

In this study we showed that a brief, transient activation of MSDB VGluT2 neurons is sufficient to drive persistent locomotion and subsequent theta oscillations in the hippocampus. Interestingly, the effect on locomotion persisted in the absence of theta activity as demonstrated by the application of a synaptic blocker cocktail (Figure 2 D-F). These results indicate that intraseptal synaptic microcircuits are necessary to maintain theta activity in the hippocampus, in line with previously published results (***Koenig et al., 2011***; ***Brandon et al., 2011***; ***Pastalkova et al., 2008***; ***Robinson et al., 2016***). However, during synaptic blockade transient activation of MSDB VGluT2 neurons lead to extended bouts of locomotion. We identify persistent firing of MSDB VGluT2 neurons as a cell-intrinsic driving force for locomotor activity.

It was previously reported (***Robinson et al., 2016***) that $\sim 2.6\%$ of MSDB VGluT2 neurons project to the hippocampus. However, despite the reported functional connectivity, the stimulation of VGluT2 axons in fimbria fornix did not lead to theta induction. In our previous work (***Fuhrmann et al., 2015***), we showed a disinhibitory mechanism that facilitates the synaptic integration of Schaffer collateral and perforant path input by CA1 pyramidal neurons depended on the activity rates of MSDB VGluT2 neurons. Taken together, these results indicate that, although the activation of MSDB VGluT2 terminals in the hippocampus is not sufficient to induce hippocampal theta activity, this activity might be modulated through disinhibition of the two main inputs to the CA1 hippocampal region, possibly by a different subpopulation of MSDB VGluT2 neurons than the ones driving locomotion. In addition, activation of VGluT2 neurons could be the source of tonic excitation of parvalbumin-positive interneurons, that in turn drive theta rhythm, as shown recently (***Kocsis et al., 2021***).

Using a transient single pulse, 1s light stimulation of MSDB VGluT2 neurons, we first observed locomotion initiation followed by the appearance of theta activity (Figure 1E). It was previously reported that theta oscillations either appear simultaneously with the locomotion onset (***Teitelbaum et al., 1975***) or several hundred miliseconds before, and that its frequency could predict the vigour of the subsequent movement (***Green and Arduini, 1954***; ***Vanderwolf, 1969***; ***Whishaw and Vanderwolf, 1973***; ***Bland et al., 2006***). We also previously showed (***Fuhrmann et al., 2015***) using a theta-rhythmic MSDB VGluT2 stimulation that theta activity precedes the locomotion, but that the duration from stimulation to locomotion onset depended on the firing frequency of MSDB VGluT2 neurons. The fact that in response to brief transient stimulation locomotion initiation preceded the onset of theta

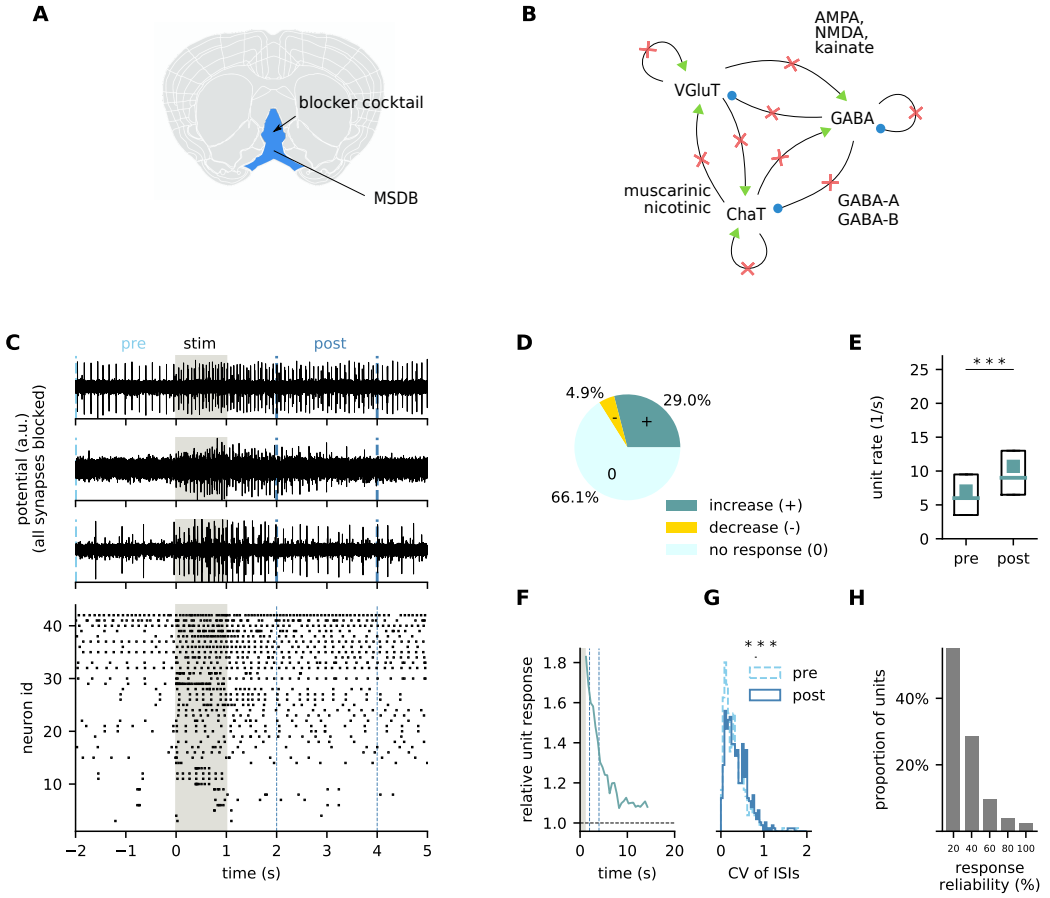

Figure 4. Persistent activity is generated by intrinsic dynamics of MSDB VGluT2 neurons
A. Application of the blocker cocktail to the MSDB. Produced using The Scalable Brain Atlas (***Bezgin et al., 2009***), based on The Allen Reference Atlas (***Lein et al., 2007***). **B.** Types of synapses blocked by the blocker cocktail. Excitatory synapses are marked by green arrows and inhibitory by blue circles. **C.** Representative traces of the extracellular potential in an acute MSDB slice preparation. The grey vertical bands mark the continuous light stimulus (upper panel). Extracted single-unit activity for one representative slice (lower panel). **D.** Percentages of units with significant increase (dark green), significant decrease (yellow) and no significant change (light green) of firing rate in response to the stimulus. For significance of a single-unit response to one stimulus repetition, $p < 0.05$ from the one-sided Mann-Whitney U-test applied on pre- and post-stimulus inter-spike intervals was required (pre: $(-2, 0)$ s, post: $(2, 4)$ s). **E.** Distribution of firing rates before and after the stimulus (pre: $(-2, 0)$ s, post: $(2, 4)$ s). Only units with persistent activity were considered. Statistical significance of the difference between pooled mean firing rates pre and post: $p = 2.3 \cdot 10^{-31}$ (185 trials). **F.** Trial-averaged time course of single-unit spiking activity. Single stimulus response per unit. **G.** Distribution of coefficients of variation (CV) or inter-spike intervals (ISIs), pre stimulus ($(-2, 0)$ s, blue) and post stimulus ($(2, 4)$ s, red). Single stimulus response per unit. **H.** Percentages of units that respond with given reliability across five stimulus repetitions. Statistical significance was calculated using the two-sided Wilcoxon's signed-rank test. 11 brain slices were used.

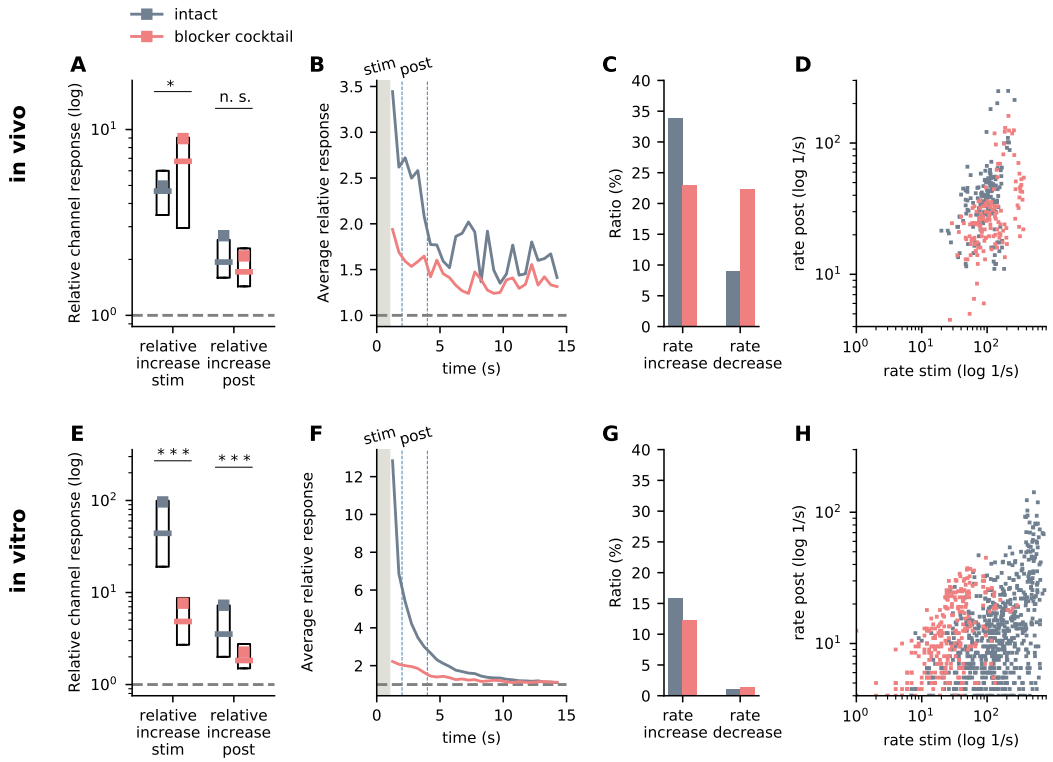

Figure 5. MSDB network increased the strength of firing response.
A. Relative rate response during and after the stimulus in the intact network (blue-grey) and with the blocker cocktail (pink). The relative rate response during (resp. after) the stimulus was calculated as the mean firing rate during the stimulus (resp. in the interval $(2, 4)$ s) divided by the baseline calculated over 2 seconds prior to the stimulus in each channel. Numbers of trials: 56 in vivo intact, 33 in vivo blocker cocktail. Statistical significance: rate increase during the stimulus $p = 0.031$, post stimulus $p = 0.11$. The bar denotes the median, the square the mean and the box spans between the first and the third quartile. Statistical significance was calculated using the two-sided Mann-Whitney U-test. **B.** Trial-averaged instantaneous firing rate of the MSDB population divided by the pre-stimulus baseline. **C.** Percentages of channels where a significant increase, resp. decrease was observed compared to pre-stimulus baseline. Significance of rate increase or decrease in each channel was calculated using the one-sided Mann-Whitney U-test. **D.** Relationship between the multi-unit firing rate during (horizontal axis) and in the interval $(2, 4)$ s (vertical axis). **E.** As A in the acute MSDB slice preparation. Numbers of trials: 261 from 19 intact slices, 83 from 11 slices with blocker cocktail. Statistical significance: rate increase during the stimulus $p = 4 \cdot 10^{-30}$, post stimulus $p = 6 \cdot 10^{-12}$. **E-H.** As B,C in the acute MSDB slice preparation.

power could be explained by the high frequency firing of MSDB neurons during the 1s continuous stimulus (Figure 5A).

While we provide evidence that under synaptic intraseptal blockade MSDB VGluT2 neurons drive locomotion while theta oscillations are blocked, it remains unknown whether behavioural or cognitive performance is impaired. Theta oscillations have clearly documented mnemonic functions. Previous studies showed that septal inhibition and the following loss of hippocampal theta leads to spatial memory deficits (***Winson, 1978***), dissociation of grid cell periodicity (***Brandon et al., 2011***; ***Koenig et al., 2011***) and internally generated hippocampal firing fields (***Pastalkova et al., 2008***; ***Wang et al., 2015***). In addition, a recent study (***Bolding et al., 2020***) demonstrated that theta activity is not necessary for location-specific firing of hippocampal cells, but that place cell activity requires septal circuits to support accurate navigation. Another open question is the motivation for animal's movement induced by the activation of MSDB VGluT2 neurons. Animals' movements can be driven by different motivations that support survival in the nature – exploration of cues and environments, fight, flight, sexual and parental behaviour. Increasing research evidence (***Zhang et al., 2018***) is pointing to the role of MSDB networks in several of above mentioned behaviours. Given that we observe reliable locomotion induction by stimulating MSDB VGluT2 neurons, even when the MSDB network is inhibited, these results suggest that MSDB VGluT2 neurons send their projections to other brain regions that connect MSDB to the motor circuits. Future studies are required to elucidate which brain regions receiving MSDB VGluT2 inputs underlie the locomotion promoting effects as well as a motivation for the induced movements.

Persistent firing has been suggested to represent the active neural mechanism through which the brain stores information and thus supports working memory (as opposed to the passive mechanism, for a review see ***Barak and Tsodyks, 2014***). However, several studies reported that the role of persistent activity may go beyond the working memory, including reinforcement learning, decision making and innate defensive behaviour (***Seo et al., 2007***; ***Barraclough et al., 2004***; ***Seo et al., 2009***; ***Histed et al., 2009***; ***Kennedy et al., 2020***). There is compelling evidence of the MSDB circuits being involved in several of these functions, including operant reward learning (***Vega-Flores et al., 2013***), working memory (***Turnbull et al., 1994***; ***McNaughton et al., 2006***; ***Lipponen et al., 2012***; ***Roland et al., 2014***; ***Li et al., 2020***) and decision making (***Collins and Saunders, 2019***). Thus, future studies should elucidate the behavioural causal role of the MSDB VgluT2 neurons persistent activity.

Both the intrinsic biophysical properties of individual cells as well as synaptic circuit properties were shown to be mechanistically involved in persistent activity. The evidence of intrinsic cellular conductances being involved in generating persistent activity originates from an extensive body of literature (***Fransén et al., 2006***; ***Pressler and Strowbridge, 2006***; ***Navaroli et al., 2012***; ***Jochems and Yoshida, 2015***; ***Knauer et al., 2013***), where it was reported that a transient intracellular depolarization leads to persistent firing in specific neurons, even when synaptic transmission is pharmacologically blocked. Most of these studies conducted experiments under application of carbachol (muscarinic receptor agonist), that is postulated to mimic the elevated increase of acetylcholine during increased attention linked to working memory. Other studies reported the necessity of synaptic circuits to drive persistent activity (***Inagaki et al., 2019***; ***Hart and Huk, 2020***), further supported by numerous computational models of persistent activity based on attractor networks (***Amit and Brunel, 1997***; ***Barak and Tsodyks, 2007***; ***Nachstedt and Tetzlaff, 2017***; ***Compte, 2006***; ***Zylberberg and Strowbridge, 2017***). Here, we observe prominent persistent activity following the transient stimulation of MSDB VGluT2 neurons, even with application of synaptic blockers and without additional application of carbachol. This implies that MSDB VGluT2 neurons are equipped with biophysical properties that enable them to exhibit intrinsic persistent firing. However, we did observe more prominent persistent firing in the intact network condition, indicating that the network amplifies the prominence of the sustained firing. As was demonstrated in other preparations, the absence of spiking activity after the stimulus in some neurons (Figure 5C, G, Figure S2) may be caused by a plateau depolarization that inactivates sodium channels and thereby suppresses

action potential generation (***Tian et al., 2014***). There are at least two potential reasons why the action potential suppression was more frequently observed in the presence of synaptic blockers (Figure 5C, G). First, in the intact network the plateau depolarization may often be disrupted by recurrent inhibition. Second, the plateau depolarization caused by the activation of the metabotropic glutamate receptors (mGluRs) may be stronger in the blocked condition due to a higher concentration of glutamate in the extracellular space. Consequently, the activation of mGluRs in the intact network may lead to a subthrehold plateau depolarization, causing an increased firing rate, and to a suprathreshold plateau depolarization in the blocked network, causing the action potential suppression (***Tian et al., 2014***). Furthermore, the existence of gap junctions in MSDB has been previously reported (***Belluardo et al., 2000***; ***Garner et al., 2005***). As our blocker cocktail did not include gap junction and mGluR blockers, it is not fully ruled out that in addition to VGluT2 positive cells other MSDB neurons may also display persistent activity.

Several studies investigated the biophysical mechanisms underlying persistent activity. In many cortical neurons, it was reported that the persistent firing likely involves a second messenger that activates the underlying depolarizing response. The evidence for this type of reasoning originates from the studies showing that persistent firing is sensitive to the concentration of Ca ions (***Pressler and Strowbridge, 2006***; ***Rahman and Berger, 2011***; ***Lei et al., 2014***). While several laboratories (***Haj-Dahmane and Andrade, 1999***; ***Rahman and Berger, 2011***; ***Lei et al., 2014***; ***Tahvildari et al., 2008***; ***Zhang et al., 2011***) invested considerable efforts in studying this mechanism, the Ca-dependent current enabling the neurons to fire persistently following the stimulus still remains elusive. One suggested mechanism is a form of Ca-activated non-selective cation current (Ican) (***Pace et al., 2007***; ***Rubin et al., 2009***). Several groups reported that specific subtypes of transient receptor potential canonical (TRPC) channels may mediate Ican responses in cortical neurons (***Yan et al., 2009***; ***Zhang et al., 2011***; ***Reboreda et al., 2011***; ***Lei et al., 2014***), while one recent study (***O'Malley et al., 2020***) showed the involvement of TRPM channels in persistent firing displayed by thalamic reticular nucleus neurons. Future studies should address the specific biophysical mechanisms underlying the capability of MSDB VGluT2 neurons to fire persistently. While investigating the intrinsic mechanisms and conductances underlying the MSDB persistent firing we discovered are without the scope of this study, it is of highest interest given the diversity of the behavioural and cognitive functions MSDB is involved in.

Taken together, this study is shedding novel light on the under-explored glutamatergic neurons in MSDB and adding to the increasing number of studies showing of the role of the MSDB networks beyond the pacemaking of theta oscillations.

Materials and Methods

Transgenic mice

Experiments were performed in adult female VGluT2-cre mice Slc17a6$^{tm2(cre)Lowl}$/J, (The Jackson Laboratory, Bar Harbor, ME USA). Mice were group-housed under specific pathogen-free conditions with 12-hour dark and light cycle before and after the virus injection, and kept single-housed after the chronic surgery for in vivo experiments. All experiments were performed in the light phase of the cycle. Ab libitum food and water was provided. All experimental procedures were approved by the local authorities of North Rhine-Westphalia and performed in accordance with DZNE regulations in agreement with European Committees Council Directive.

Virus injection

Stereotactic injection of adeno-associated virus (AAV) was performed as described previously in detail (***Fuhrmann et al., 2015***; ***Justus et al., 2017***). In brief, mice were anesthetized and head-fixed on a stereotactic frame. A small craniotomy was drilled above the medial septum (+1.0 mm anterior-posterior and +0.7 mm lateral, relative to bregma, stereotactic coordinates from ***Franklin and Paxinos 2008***). Channelrhodopsin-virus (pAAV2.1-EF1a-double floxed ChR2-EYFP-WPR (H134R), 1 µl)

was injected into each of two loci of the medial septum (-4.6 mm and -4.2 mm ventral, relative to bregma, angled 10° laterally) through the small craniotomy at 0.1 µl/min. Surgery for in vivo tetrode recordings followed 7 weeks after AAV injection.

In Vivo Experimental Procedures

Surgery

Chronic surgery was performed as described previously (***Justus et al., 2017***). A fiber-optic cannula (OFC_400/430 0.37_5mm_SM3(P)_FLT, Doric Lenses, Quebec, Canada) was implanted rostrocaudally, angled $38°$ ventrally and $10°$ laterally. The MSDB was approached for 5.5 mm. Monopolar field potential electrode was positioned into hippocampal stratum radiatum (-2.0 mm anterior-posterior, -2.0 mm lateral and -1.6 mm ventral, relative to bregma). A 1.0 mm of craniotomy for tetrode recording in MS was drilled on the right hemisphere ($+1.0$ mm anterior-posterior and $+0.7$ mm lateral from bregma). For awake head-fixation a small metal-bar (Luigs-Neumann, Ratingen, Germany) was placed paramedian on the skull. Animals were allowed to recover for 2 weeks.

Recording

Mouse was head fixed onto a spherical treadmill (material: styrofoam, diameter: 20 cm) which only rotates in a straight direction or a linear treadmill (length: 200 cm, width: 7 cm, color: black, no cue) with virtual reality environment. The running speed was detected by an optical computer mouse. Either a single or a double shank tetrode (0.5 – 0.8 MΩ, Thomas RECORDING GmbH, Gießen, Germany) was glued to 34G cannula and lowered to medial septum through the craniotomy in a depth between 3400 and 4300 µm from brain surface with an angle of 10° laterally. Multi-unit recording was performed with reference mode and filtered with $500\lambda2000$ Hz bandpass filter using a 16 channels extracellular amplifier (EXT-16DX, npi, Tamm, Germany). LFP was filtered with $3\lambda700$ Hz bandpass filter and recorded using an extracellular amplifier (EXT-02F/2, npi, Tamm, Germany). Together with an analog-converted position readout, the single units and LFP were sampled at 25 kHz using an ITC-18 interface (HEKA Elektronik, Lambrecht, Germany) and recorded by a custom written software in Igor Pro 6.3 (WaveMetrics, Portland, USA). A 488 nm diode laser (Excelsior-488C-200-CDRH, Spectra-Physics, Santa Clara, USA) was used for the light stimulation. The blockers were applied using a UltraMicroPump with Hamilton syringe (Word Precision Instruments, Berlin, Germany) via the 34G cannula.

In Vitro Experimental Procedures

Slice preparation

For MEA recordings of spontaneous action potentials, 400 µm thick MSDB slices were prepared as described previously (***Fuhrmann et al., 2015***). After cutting, slices were transferred to an interface chamber (Warner Instruments, Hamden, USA) containing ACSF (***Maier et al., 2009***) for recovery (mM): 119 NaCl, 2.5 KCl, 2.5 $CaCl_2$, 1.0 NaH_2PO_4, 26 $NaHCO_3$, 1.3 $MgCl_2$, 10 glucose, oxygenated with 95% O_2 and 5% CO_2. MSDB slices were kept inside the interface chamber on lens cleaning tissue (Grade 105, Whatman, Maidenstone, England) allowing optimal oxygenation due to a laminar flow of preheated ($35°$C) ACSF above and underneath the slices for at least 3 hours. In total 19 slices were used in the intact condition, 11 with NBQX, D-AP5 and 11 with the blocker cocktail.

Microelectrode Array (MEA) recordings

Extracellular waveforms in the MSDB slices in VGluT2-cre mice were recorded with a MEA2100-System (Multi Channel Systems, Reutlingen, Germany, RRID:SCR_014809) on 60pMEA100/30iR-Ti MEAs with round titanium nitride (TiN) electrodes, as described in ***Sosulina et al.*** (***2021***). In detail, the MS slices was positioned onto a 6×10 matrix of electrodes, with a spacing of 100 µm and an electrode diameter of 30 µm. ACSF temperature was adjusted to 35°C using a heatable perfusion cannula PH01 together with a TC01 controlling unit (Multi Channel Systems, Reutlingen, Germany). The position of the slice was stabilized by applying of a constant negative pressure of 25 – 30 mBar.

Data were acquired with MC_Rack (V 4.5.16.0, Multi Channel Systems, Reutlingen, Germany) at 25 kHz sampling rate with an MEA2100-lite-Interface Board.

Optogenetic stimulation in MSDB brain slices

Brain slices of VGluT2-cre mice expressing channelrhodopsin in the MSDB were used for optogenetic experiments. Optogenetic stimulation in slices was performed with a light fiber coupled 473 nm diode laser (LuxX473-80, Omicron-Laserage). The light fiber tip was placed in a distance of ≤ 5 mm to the slice. Five repetitions of continuous stimulation with 1 second duration were applied. Optogenetic stimulation was repeated under changed pharmacological conditions: first, with glutamatergic blockers NBQX (10 μM) and DAP5 (50 μM), followed by glutamatergic blockers together with GABA-ergic blockers SR-95531 (10 μM), CGP52432 (1 μM) and cholinergic blockers Atropin (10 μM), MLA (200nM).

Data analysis

Software

Data analysis was performed using custom-written scripts in Python v3.6.10, with the packages Numpy v1.19.2, Scipy v1.5.2, Neo v0.7.1, Elephant v0.6.2 and Matplotlib v3.3.2. Single units were isolated from extracellular potentials using Mountainsort v3 (***Barnett et al., 2016***).

Speed

The speed was calculated by differentiating the position down-sampled to 1 ms (0.2 ms in Figures 1F, 2E, S4E and S3). Then it was low-pass filtered at 20 Hz using the Butterworth filter of order 5. To be able to test movement initiation in response to the optical stimulus, data sets where the average speed of the mouse within 3 s before the stimulus was higher than 3 cm/s were discarded. A running phase was defined as a continuous time interval with minimal duration of 1 s, when the speed doesn't go below 3 cm/s for more than 1 s.

Spectrograms

The spectrograms were computed using Fourier analysis with frequency resolution 2 Hz and 62.5 ms overlap of 500 ms time intervals. Average power in the theta frequency range was calculated as an average of wavelets centered around frequencies $7, 7.5, 8, \ldots, 12$ Hz from signal downsampled to 5000 Hz.

Spiking activity

Single-unit activity was extracted using Mountainsort v3 (***Barnett et al., 2016***) with clip size corresponding to a 2ms window, isolation threshold for curation 0.85, noise overlap 0.03 and threshold 7. To extract the multi-unit activity, the signal was first band-pass filtered between 300 Hz and 3000 Hz using the Butterworth filter of order 5. Action potential peaks were then extracted using Elephant v0.6.2 by thresholding with the threshold set to 3, resp. 4.5 times the standard deviation of the band-pass filtered signal in vivo, resp. in vitro. Histograms of spiking activity were calculated by binning the spikes into 200 ms bins. For the in vitro single unit analysis, only units with minimum of 10 spikes were considered for analysis.

Persistent activity was defined as significantly increased firing rate in the time interval 1–3 s after the stimulus offset (i.e. 2–4 s after the stimulus onset), compared to baseline calculated over 2 s before the stimulus onset (as described above, the data where the mouse was running before the stimulus was discarded). The activity in the first second after the stimulus offset was not considered as some units in the slice preparation showed elevated firing only within the first second after the stimulus offset, indicating prolonged stimulus response rather than intrinsically generated persistent activity. Pre- and post-stimulus firing rate was calculated as the average firing rate over the respective intervals $(-2, 0)$s and $(2, 4)$s relatively to the stimulus onset. Only one channel per trial is considered for statistical analysis in Figures 1, 2, S4. In Figures 3F, 4E and S5E only the first

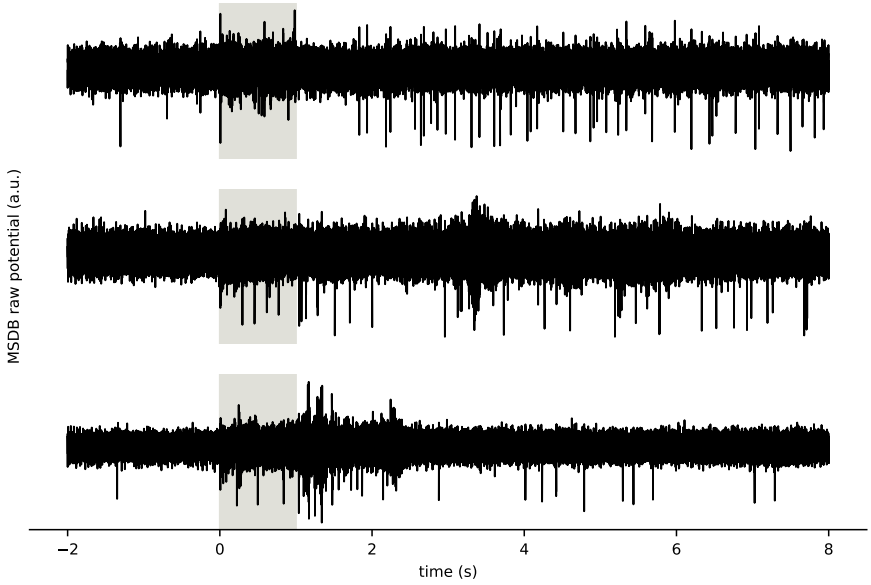

Figure S1. Examples of potential traces in vivo.
Representative traces of raw potentials from the MSDB in vivo. Stimulus period is indicated with the grey region.

stimulus realization was considered to avoid persistent activity from the previous stimulus to enter the pre-stimulus activity.

The relative firing rate response during (resp. before) the stimulus in Figure 5 was calculated as the mean firing rate during the stimulus (resp. in the interval $1-3$ seconds after the stimulus offset) divided by the mean firing rate calculated over 2 seconds prior to the stimulus.

Statistical testing

In the cases with clearly defined pairs of values (e.g. pre- and post-stimulus value of the mean firing rate), the two-sided Wilcoxon's signed-rank test was used. In all other cases the non-parametric two-sided Mann-Whitney U-test was applied, as the data were not normally distributed.

Supplements

Acknowledgments

The resources for all experiments were provided by the German Center for Neurodegenerative Diseases in Bonn (Germany). The compute resources for the handling and analysis of experimental data were provided by the Institute of Neuroscience and Medicine (INM-6) of the Jülich Research Centre (Germany). The authors received funding from the German Research Foundation (DFG), grants SFB 1089 (FL, LS, SR) and DI 1721/3-1 KFO219-TP9 (KK, TT). TT was further supported by the European Union's Horizon 2020 Framework Programme for Research and Innovation under Specific Grant Agreement No. 720270, 785907 (Human Brain Project SGA1, SGA2). KK received funding from the Charles University Primus program No. 20/MED/006SR. SM was supported by the Swedish Research Council (grant 2017-06254).

The authors are grateful to Balazs Hangya and Motoharu Yoshida for insightful comments on a previous version of the manuscript as well the members of Cellular Neuroscience and Cognition and Emotion laboratories for helpful discussions, Falko Fuhrmann for technical assistance with the experiments, Junji Ito for advice on statistical methods, and Sebastian B. C. Lehmann for help with graphical design.

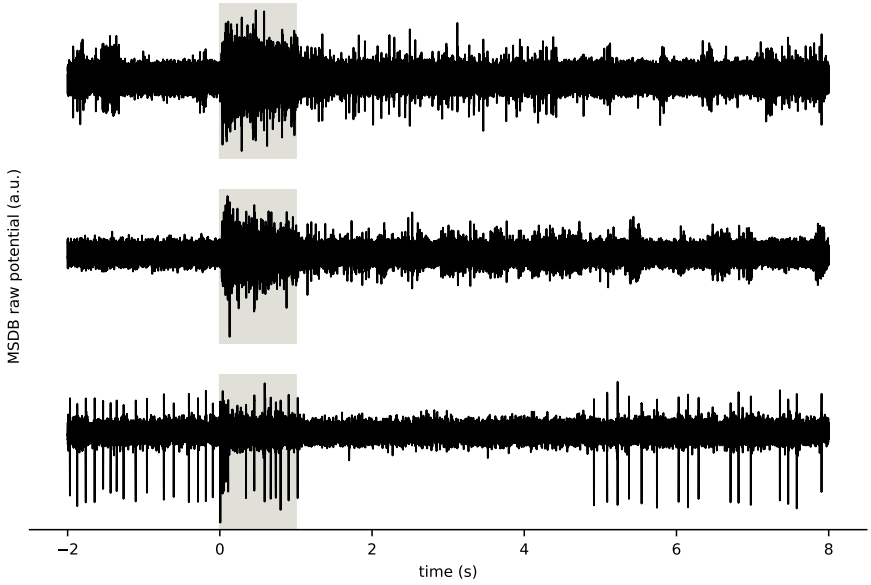

Figure S2. Examples of potential traces in vivo with blocked MS synapses.
Representative traces of raw potentials from the MSDB in vivo after the application of the blocker cocktail. With the blocker coctail cessation of activity after the stimulus was observed more often than in the intact network, see also Figures 3, 4. Stimulus period is indicated with the grey region.

Competing Interests

The authors declare no competing interests.

References

Amit DJ, Brunel N. Model of global spontaneous activity and local structured activity during delay periods in the cerebral cortex. Cerebral Cortex. 1997 4; 7:237–252. https://doi.org/10.1093/cercor/7.3.237, doi: 10.1093/cercor/7.3.237.

Barak O, Tsodyks M. Persistent activity in neural networks with dynamic synapses. PLoS Computational Biology. 2007; 3:0323–0332. https://doi.org/10.1371/journal.pcbi.0030104, doi: 10.1371/journal.pcbi.0030035.

Barak O, Tsodyks M. Working models of working memory. Current Opinion in Neurobiology. 2014 4; 25:20–24. https://doi.org/10.1016/j.conb.2013.10.008, doi: 10.1016/j.conb.2013.10.008.

Barnett AH, Magland JF, Greengard LF. Validation of neural spike sorting algorithms without ground-truth information. Journal of Neuroscience Methods. 2016 5; 264:65–77. doi: 10.1016/j.jneumeth.2016.02.022.

Barraclough DJ, Conroy ML, Lee D. Prefrontal cortex and decision making in a mixed-strategy game. Nature Neuroscience. 2004 4; 7:404–410. https://doi.org/10.1038/nn1209, doi: 10.1038/nn1209.

Belluardo N, Mudò G, Trovato-Salinaro A, Gurun SL, Charollais A, Serre-Beinier V, Amato G, Haefliger JA, Meda P, Condorelli DF. Expression of Connexin36 in the adult and developing rat brain. Brain Research. 2000 5; 865:121–138. https://doi.org/10.1016/S0006-8993(00)02300-3, doi: 10.1016/S0006-8993(00)02300-3.

Bezgin G, Reid AT, Schubert D, Kötter R. Matching spatial with ontological brain regions using java tools for visualization, database access, and integrated data analysis. Neuroinformatics. 2009 3; 7:7–22. https://scalablebrainatlas.incf.org/index.php, doi: 10.1007/s12021-008-9039-5.

Bland BH, Jackson J, Derrie-Gillespie D, Azad T, Rickhi A, Abriam J. Amplitude, frequency, and phase analysis of hippocampal theta during sensorimotor processing in a jump avoidance task. Hippocampus. 2006 8; 16:673–681. https://doi.org/10.1002/hipo.20210, doi: 10.1002/hipo.20210.

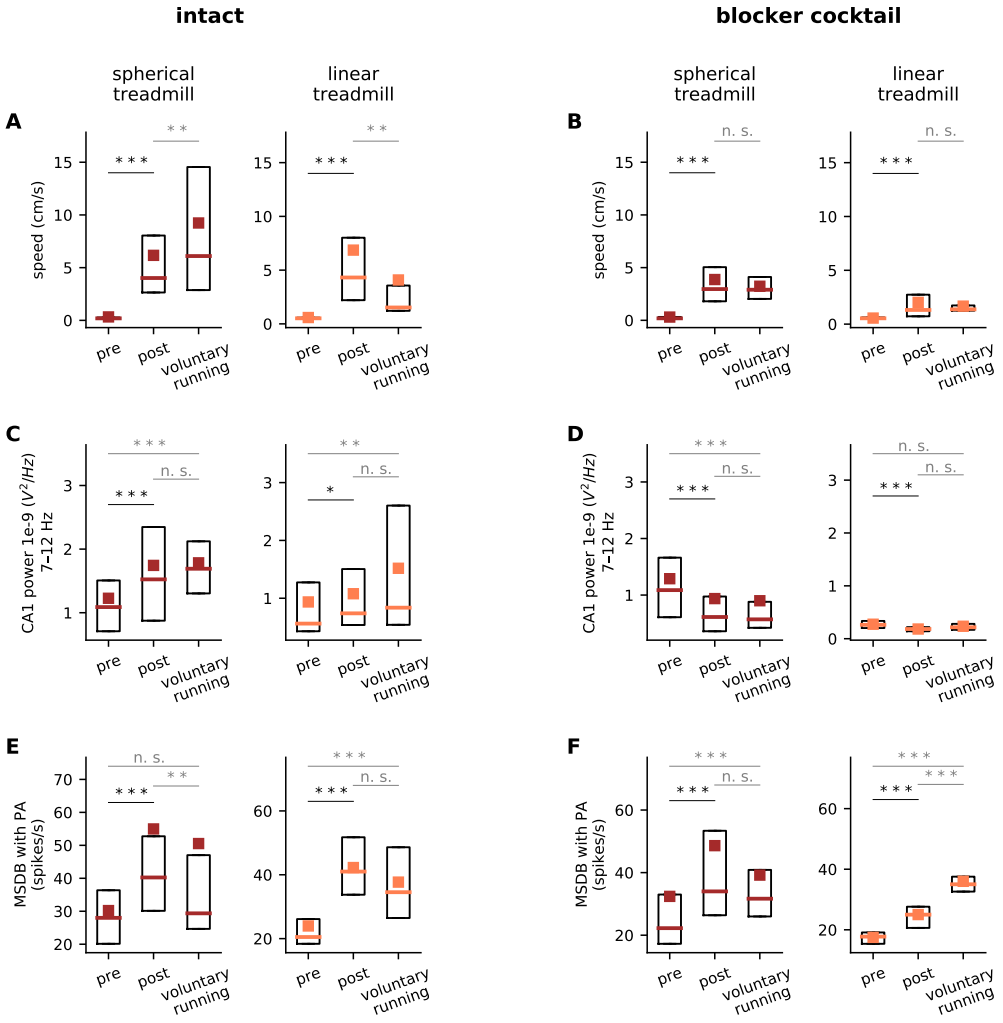

Figure S3. Comparison of results recorded on the spherical (left subcolumn) and linear treadmill (right subcolumn) pre-, post-stimulus and during voluntary running.
A. Running speed with intact MSDB network. **B.** Running speed with blocked synaptic transmission in the MSDB. **C.** Mean CA1 power in the range 7–12 Hz in the intact MSDB network. **D.** Mean CA1 power in the range 7–12 Hz with blocked synaptic transmission in the MSDB. **E.** Mean firing rate in MSDB channels with persistent activity in the intact MSDB network. **F.** Mean firing rate in MSDB channels with persistent activity with blocked synaptic transmission in the MSDB. All recordings of 4 mice in intact and 3 mice in blocked condition were used. For firing rates only one channel per mouse is considered. Statistical significance was calculated using the two-sided Wilcoxon's signed-rank test for pre- vs post-stimulus difference (black) and the two-sided Mann-Whitney U-test in other cases (grey). Numbers of trials intact on the spherical treadmill: 118 with stimulus, 75 of them with persistent activity, 83 trials with voluntary running, 45 of them with persistent activity; intact on the treadmill: 47 trials with stimulus, 44 of them with persistent activity, 38 trials with voluntary running, 34 of them with persistent activity. Blocker cocktail on the spherical treadmill: 110 with stimulus, 60 of them with persistent activity, 60 with voluntary running, 31 of them with persistent activity. Statistical significance, p-values calculated using the two-sided Wilcoxon's signed-rank test for pre- vs post-stimulus difference (black) and the two-sided Mann-Whitney U-test in other cases (grey) in the order pre vs post, post vs voluntary running, pre vs voluntary running:

	intact		blocker cocktail	
	spherical treadmill	linear treadmill	spherical treadmill	linear treadmill
speed	$\sim 10^{-21}$, 0.0098, –	$\sim 10^{-9}$, 0.002, –	$\sim 10^{-19}$, 0.9, –	$\sim 10^{-6}$, 0.6, –
CA1 power 7–12 Hz	$\sim 10^{-5}$, 0.31, $\sim 10^{-7}$	0.02, 0.16, 0.007	0.0003, 0.6, 0.0002	0.0003, 0.05, 0.18
firing rate MSDB multi-unit with PA	$\sim 10^{-14}$, 0.006, 0.074	$\sim 10^{-9}$, 0.056, $\sim 10^{-6}$	$\sim 10^{-11}$, 0.4, 0.0007	0.0004, 0.0002, $\sim 10^{-5}$

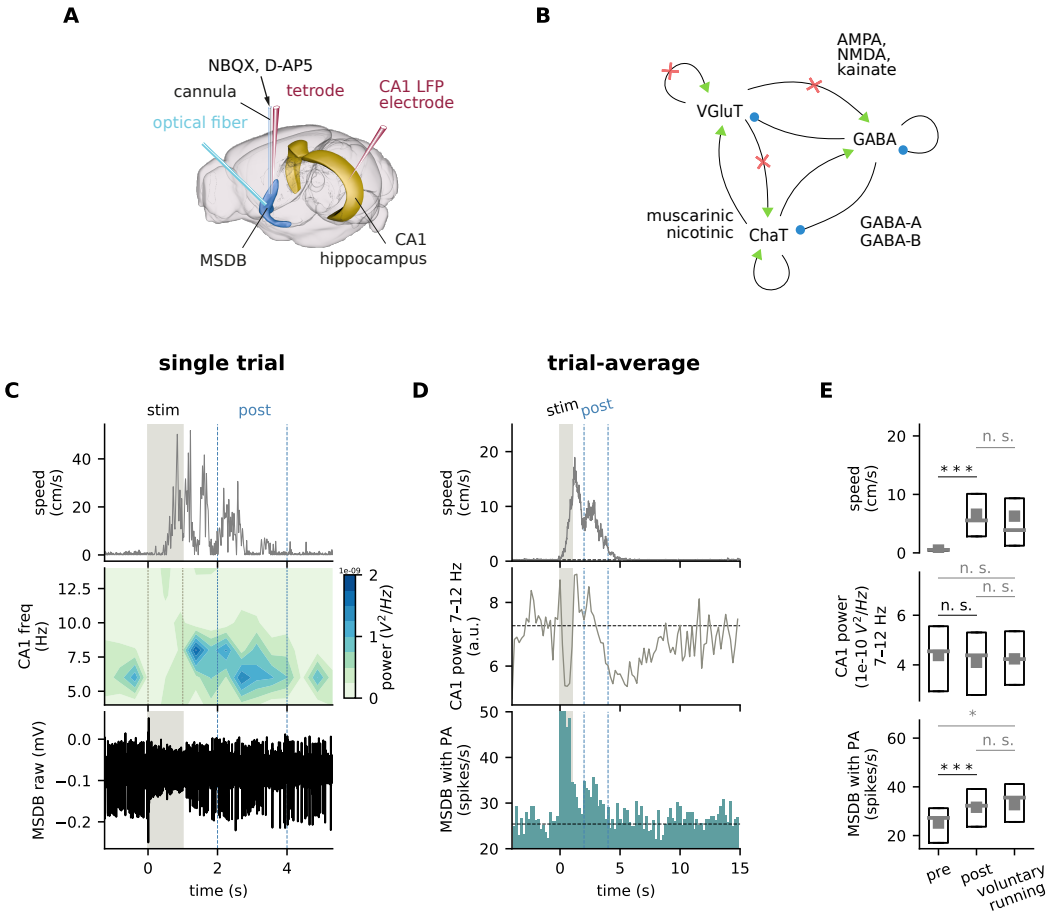

Figure S4. Stimulus response in vivo with blocked MSDB glutamatergic synapses.
A. NBQX, D-AP5 was applied through a cannula in the MSDB. Produced using The Scalable Brain Atlas (***Bezgin et al., 2009***), based on The Allen Reference Atlas (***Lein et al., 2007***). **B.** Types of synapses blocked by NBQX, D-AP5. Excitatory synapses are marked by green arrows and inhibitory by blue circles. **C.** Representative recordings of speed, CA1 LFP with the corresponding spectrogram and MSDB extracellular potential. The grey vertical band marks the continuous light stimulus (0–1s). The grey vertical band marks the continuous light stimulus (0–1 s), the dotted lines mark the time interval used to analyze post-stimulus activity (2–4 s). Same mouse as in Figure 1D. **D.** Trial-averaged speed (upper panel), CA1 LFP power in the frequency range 7–12 Hz (middle panel) and the average histogram of multi-unit spiking activity of channels with persistent activity (PA) (lower panel). Average across all recording sessions with 4 mice. For significance of a single-channel positive response to one stimulus repetition, $p < 0.05$ from the one-sided Mann-Whitney U-test applied on inter-spike intervals was required. **E.** Distribution of time-averaged speed (upper panel), CA1 LFP power in the range 7–12 Hz (middle panel) and mean firing rate of channels with PA (lower panel) for time periods when the mouse was at rest, during voluntary running, and within 2 seconds after the stimulus offset. Bar denotes the median, square the mean and the box spans between the first and the third quartile. All recordings of 2 mice were used. Numbers of trials: 47 trials with one stimulus realization, out of them 30 show persistent activity, 18 trials with voluntary running, out of them 12 show persistent activity. Statistical significance: pre- vs post-stimulus speed $p = 2.4 \cdot 10^{-9}$, post-stimulus vs voluntary running $p = 0.48$, LFP power pre vs post 0.72, post-stimulus vs voluntary running 0.88, pre-stimulus vs voluntary running $p = 0.92$, PA pre vs post $p = 1.7 \cdot 10^{-6}$, post-stimulus vs voluntary running $p = 0.73$, pre-stimulus vs voluntary running $p = 0.03$. The difference between the speed before the stimulus and during voluntary running was significant by construction. Statistical significance was calculated using the two-sided Wilcoxon's signed-rank test for pre- vs post-stimulus difference (black) and the two-sided Mann-Whitney U-test in other cases (grey).

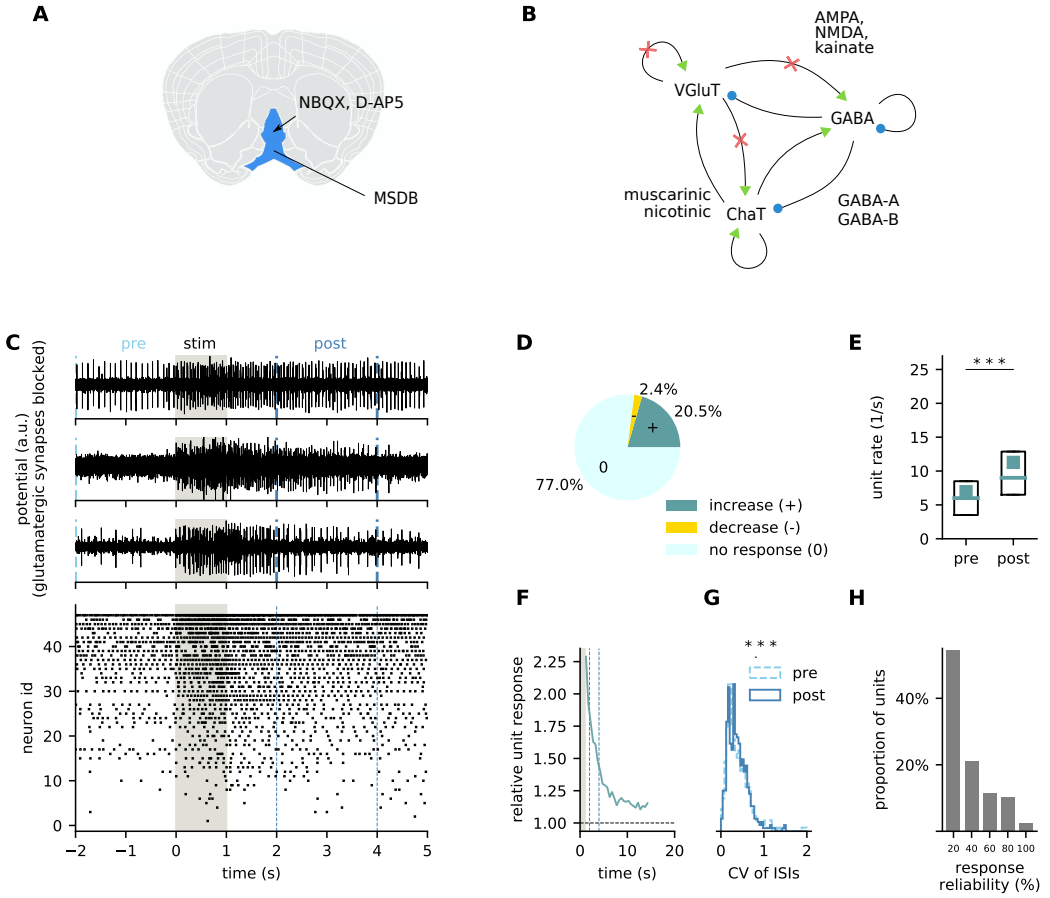

Figure S5. Single-unit response to stimulus in vitro with blocked MSDB glutamatergic synapses. **A.** Application of NBQX, D-AP5 to the MSDB. Produced using The Scalable Brain Atlas (***Bezgin et al., 2009***), based on the Allen Reference Atlas (***Lein et al., 2007***). **B.** Types of synapses blocked by NBQX, D-AP5. Excitatory synapses are marked by green arrows and inhibitory by blue circles. **C.** Representative traces of the extracellular potential in the acute MSDB slice preparation. The grey vertical bands mark the continuous light stimulus (upper panel). Extracted single-unit activity for one representative slice (lower panel). **D.** Percentages of units with significant increase (dark green), significant decrease (yellow) and no significant change (light green) of firing rate. For significance of a single-unit response to one stimulus repetition, $p < 0.05$ from the one-sided Mann-Whitney U-test applied on inter-spike intervals was required. **E.** Distribution of firing rates before and after the stimulus (pre: $(-2, 0)$ s, post: $(2, 4)$ s). Only units with significantly elevated post-stimulus firing rate were considered. Statistical significance of the difference between pooled mean firing rates pre and post: $p = 7.3 \cdot 10^{-29}$ (171 trials, second stimulus repetition out of five). **F.** Trial-averaged time course of single-unit spiking activity. Single stimulus response per unit. **G.** Distribution of coefficients of variation (CV) or inter-spike intervals (ISIs), pre stimulus ($(-2, 0)$ s, blue) and post stimulus ($(2, 4)$ s, red). Single stimulus response per unit. **H.** Percentages of units that respond with given reliability across five stimulus repetitions. Statistical significance was calculated using the two-sided Wilcoxon's signed-rank test. 13 brain slices were used.

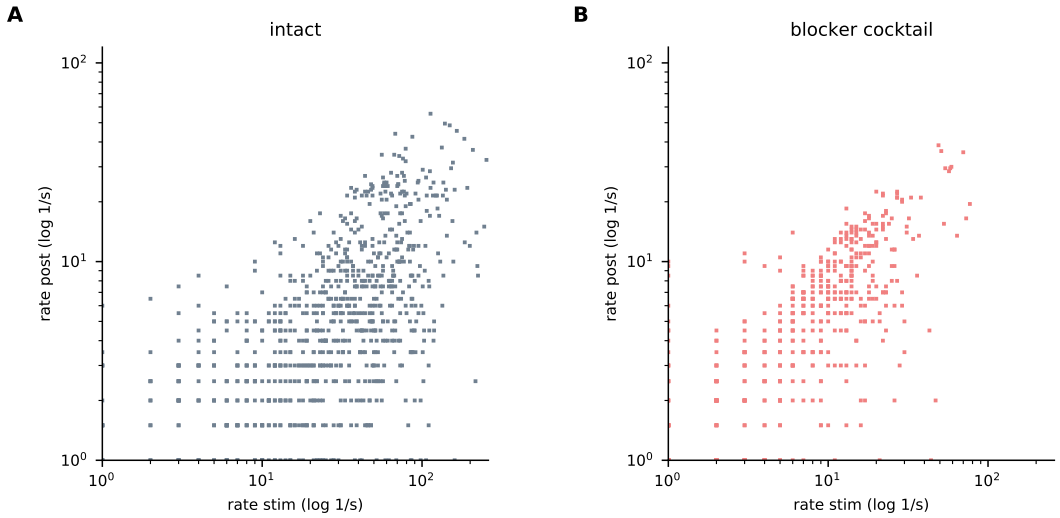

Figure S6. Relationship between the single-unit firing rate during and after the stimulus in vitro. **A.** Single unit firing rate during the stimulus (horizontal axis) and in the time interval $(2, 4)$ s (vertical axis) in the acute MSDB slice preparation. **B.** As A with blocked synaptic transmission in the MSDB.

Bolding KA, Ferbinteanu J, Fox SE, Muller RU. Place cell firing cannot support navigation without intact septal circuits. Hippocampus. 2020 3; 30:175–191. https://doi.org/10.1002/hipo.23136, doi: 10.1002/hipo.23136.

Branco T, Costa G, SciDraw | About; 2020. https://scidraw.io/about/, doi: 10.5281/zenodo.3926079.

Brandon MP, Bogaard AR, Libby CP, Connerney MA, Gupta K, Hasselmo ME. Reduction of theta rhythm dissociates grid cell spatial periodicity from directional tuning. Science. 2011 4; 332:595–599. https://science.sciencemag.org/content/332/6029/595, doi: 10.1126/science.1201652.

Brashear HR, Zaborszky L, Heimer L. Distribution of gabaergic and cholinergic neurons in the rat diagonal band. Neuroscience. 1986 2; 17:439–451. https://doi.org/10.1016/0306-4522(86)90258-7, doi: 10.1016/0306-4522(86)90258-7.

Buzsáki G. Theta Oscillations in the Hippocampus Review. Neuron. 2002; 33:325–340. https://doi.org/10.1016/S0896-6273(02)00586-X, doi: 10.1016/S0896-6273(02)00586-X.

Collins AL, Saunders BT. Brain reward network effects underlie septo-hippocampal control of flexible decision making. Neuropsychopharmacology. 2019 12; 44:2153–2154. https://doi.org/10.1038/s41386-019-0487-4, doi: 10.1038/s41386-019-0487-4.

Compte A. Computational and in vitro studies of persistent activity: Edging towards cellular and synaptic mechanisms of working memory. Neuroscience. 2006 4; 139:135–151. https://doi.org/10.1016/j.neuroscience.2005.06.011, doi: 10.1016/j.neuroscience.2005.06.011.

Dannenberg H, Kelley C, Hoyland A, Monaghan CK, Hasselmo ME. The firing rate speed code of entorhinal speed cells differs across behaviorally relevant time scales and does not depend on medial septum inputs. Journal of Neuroscience. 2019 5; 39:3434–3453. https://doi.org/10.1523/JNEUROSCI.1450-18.2019, doi: 10.1523/JNEUROSCI.1450-18.2019.

Egorov AV, Unsicker K, von Bohlen und Halbach O. Muscarinic control of graded persistent activity in lateral amygdala neurons. European Journal of Neuroscience. 2006 12; 24:3183–3194. http://doi.wiley.com/10.1111/j.1460-9568.2006.05200.x, doi: 10.1111/j.1460-9568.2006.05200.x.

Franklin K, Paxinos G. The Mouse Brain in Stereotaxic Coordinates. Academic Press, Elsevier; 2008.

Fransén E, Tahvildari B, Egorov AV, Hasselmo ME, Alonso AA. Mechanism of graded persistent cellular activity of entorhinal cortex layer V neurons. Neuron. 2006 3; 49:735–746. https://doi.org/10.1016/j.neuron.2006.01.036, doi: 10.1016/j.neuron.2006.01.036.

Fuhrmann F, Justus D, Sosulina L, Kaneko H, Beutel T, Friedrichs D, Schoch S, Schwarz M, Fuhrmann M, Remy S. Locomotion, Theta Oscillations, and the Speed-Correlated Firing of Hippocampal Neurons Are Controlled by a Medial Septal Glutamatergic Circuit. Neuron. 2015; 86:1253–1264. http://dx.doi.org/10.1016/j.neuron.2015.05.001, doi: 10.1016/j.neuron.2015.05.001.

Fuster JM. Unit activity in prefrontal cortex during delayed-response performance: neuronal correlates of transient memory. Journal of neurophysiology. 1973; 36:61–78. doi: 10.1152/jn.1973.36.1.61.

Garner HL, Whittington MA, Henderson Z. Induction by kainate of theta frequency rhythmic activity in the rat medial septum-diagonal band complex in vitro. Journal of Physiology. 2005 4; 564:83–102. doi: 10.1113/jphysiol.2004.080622.

Gottlieb Y, Vaadia E, Abeles M. Single unit activity in the auditory cortex of a monkey performing a short term memory task. Experimental Brain Research. 1989 1; 74:139–148. https://link.springer.com/article/10.1007/BF00248287, doi: 10.1007/BF00248287.

Green JD, Arduini AA. Hippocampal electrical activity in arousal. Journal of neurophysiology. 1954 11; 17:533–557. https://doi.org/10.1152/jn.1954.17.6.533, doi: 10.1152/jn.1954.17.6.533.

Haj-Dahmane S, Andrade R. Muscarinic receptors regulate two different calcium-dependent non-selective cation currents in rat prefrontal cortex. European Journal of Neuroscience. 1999 6; 11:1973–1980. http://doi.wiley.com/10.1046/j.1460-9568.1999.00612.x, doi: 10.1046/j.1460-9568.1999.00612.x.

Hart E, Huk AC. Recurrent circuit dynamics underlie persistent activity in the macaque frontoparietal network. eLife. 2020 5; 9:1–22. https://elifesciences.org/articles/52460, doi: 10.7554/eLife.52460.

Harvey CD, Coen P, Tank DW. Choice-specific sequences in parietal cortex during a virtual-navigation decision task. Nature. 2012 4; 484:62–68. https://www.nature.com/articles/nature10918, doi: 10.1038/nature10918.

Histed MH, Pasupathy A, Miller EK. Learning Substrates in the Primate Prefrontal Cortex and Striatum: Sustained Activity Related to Successful Actions. Neuron. 2009 7; 63:244–253. https://doi.org/10.1016/j.neuron.2009.06.019, doi: 10.1016/j.neuron.2009.06.019.

Huh CYL, Goutagny R, Williams S. Glutamatergic Neurons of the Mouse Medial Septum and Diagonal Band of Broca Synaptically Drive Hippocampal Pyramidal Cells: Relevance for Hippocampal Theta Rhythm. Journal of Neuroscience. 2010 11; 30:15951–15961. https://doi.org/10.1523/JNEUROSCI.3663-10.2010, doi: 10.1523/JNEUROSCI.3663-10.2010.

Inagaki HK, Fontolan L, Romani S, Svoboda K. Discrete attractor dynamics underlies persistent activity in the frontal cortex. Nature. 2019 2; 566:212–217. https://doi.org/10.1038/s41586-019-0919-7, doi: 10.1038/s41586-019-0919-7.

Jochems A, Yoshida M. Persistent firing supported by an intrinsic cellular mechanism in hippocampal CA3 pyramidal cells. European Journal of Neuroscience. 2013 May; 38(2):2250–2259. https://doi.org/10.1111/ejn.12236, doi: 10.1111/ejn.12236.

Jochems A, Yoshida M. A Robust In Vivo-Like Persistent Firing Supported by a Hybrid of Intracellular and Synaptic Mechanisms. PLOS ONE. 2015 4; 10:e0123799. https://dx.plos.org/10.1371/journal.pone.0123799, doi: 10.1371/journal.pone.0123799.

Justus D, Dalügge D, Bothe S, Fuhrmann F, Hannes C, Kaneko H, Friedrichs D, Sosulina L, Schwarz I, Elliott DA, Schoch S, Bradke F, Schwarz MK, Remy S. Glutamatergic synaptic integration of locomotion speed via septoentorhinal projections. Nature Neuroscience. 2017; 20:16–19. https://www.nature.com/articles/nn.4447, doi: 10.1038/nn.4447.

Kennedy A, Kunwar PS, yun Li L, Stagkourakis S, Wagenaar DA, Anderson DJ. Stimulus-specific hypothalamic encoding of a persistent defensive state. Nature. 2020 10; 586:730–734. https://doi.org/10.1038/s41586-020-2728-4, doi: 10.1038/s41586-020-2728-4.

Kiehn O, Eken T. Functional role of plateau potentials in vertebrate motor neurons. Current Opinion in Neurobiology. 1998; 8(6):746–752. https://doi.org/10.1016/S0959-4388(98)80117-7, doi: 10.1016/S0959-4388(98)80117-7.

Knauer B, Jochems A, Valero-Aracama MJ, Yoshida M. Long-lasting intrinsic persistent firing in rat CA1 pyramidal cells: A possible mechanism for active maintenance of memory. Hippocampus. 2013 9; 23:820–831. http://doi.wiley.com/10.1002/hipo.22136, doi: 10.1002/hipo.22136.

Kocsis B, Martínez-Bellver S, Fiáth R, Domonkos A, Sviatkó K, Barthó P, Freund TF, Ulbert I, Káli S, Varga V, Hangya B. Huygens synchronization of medial septal pacemaker neurons generates hippocampal theta oscillation. bioRxiv. 2021 1; p. 2021.01.22.427736. https://doi.org/10.1101/2021.01.22.427736, doi: 10.1101/2021.01.22.427736.

Koenig J, Linder AN, Leutgeb JK, Leutgeb S. The spatial periodicity of grid cells is not sustained during reduced theta oscillations. Science. 2011 4; 332:592–595. https://science.sciencemag.org/content/332/6029/592, doi: 10.1126/science.1201685.

Kubota K, Iwamoto T, Suzuki H. Visuokinetic activities of primate prefrontal neurons during delayed response performance. Journal of Neurophysiology. 1974; 37:1197–1212. https://doi.org/10.1152/jn.1974.37.6.1197, doi: 10.1152/jn.1974.37.6.1197.

Leao RN, Targino ZH, Colom LV, Fisahn A. Interconnection and Synchronization of Neuronal Populations in the Mouse Medial Septum/Diagonal Band of Brocca. Journal of neurophysiology. 2015; 1986:jn.00367.2014. https://doi.org/10.1152/jn.00367.2014, doi: 10.1152/jn.00367.2014.

Lei YT, Thuault SJ, Launay P, Margolskee RF, Kandel ER, Siegelbaum SA. Differential contribution of TRPM4 and TRPM5 nonselective cation channels to the slow afterdepolarization in mouse prefrontal cortex neurons. Frontiers in Cellular Neuroscience. 2014 9; 8:267. https://doi.org/10.3389/fncel.2014.00267, doi: 10.3389/fncel.2014.00267.

Lein ES, Hawrylycz MJ, Ao N, Ayres M, Bensinger A, Bernard A, Boe AF, Boguski MS, Brockway KS, Byrnes EJ, Chen L, Chen L, Chen TM, Chin MC, Chong J, Crook BE, Czaplinska A, Dang CN, Datta S, Dee NR, et al. Genome-wide atlas of gene expression in the adult mouse brain. Nature. 2007 1; 445:168–176. https://www.nature.com/articles/nature05453, doi: 10.1038/nature05453.

Li S, Zhou X, Constantinidis C, Qi XL. Plasticity of Persistent Activity and Its Constraints. Frontiers in Neural Circuits. 2020 5; 14. https://doi.org/10.3389/fncir.2020.00015, doi: 10.3389/fncir.2020.00015.

Lipponen A, Woldemichael BT, Gurevicius K, Tanila H. Artificial Theta Stimulation Impairs Encoding of Contextual Fear Memory. PLoS ONE. 2012 11; 7:e48506. https://dx.plos.org/10.1371/journal.pone.0048506, doi: 10.1371/journal.pone.0048506.

MacDonald CJ, Lepage KQ, Eden UT, Eichenbaum H. Hippocampal "time cells" bridge the gap in memory for discontiguous events. Neuron. 2011 8; 71:737–749. https://doi.org/10.1016/j.neuron.2011.07.012, doi: 10.1016/j.neuron.2011.07.012.

Maier N, Morris G, Johenning FW, Schmitz D. An Approach for Reliably Investigating Hippocampal Sharp Wave-Ripples In Vitro. PLoS ONE. 2009 9; 4:e6925. https://dx.plos.org/10.1371/journal.pone.0006925, doi: 10.1371/journal.pone.0006925.

Manseau F, Danik M, Williams S. A functional glutamatergic neurone network in the medial septum and diagonal band area. Journal of Physiology. 2005; 566:865–884. https://doi.org/10.1113/jphysiol.2005.089664, doi: 10.1113/jphysiol.2005.089664.

Markram H, Segal M. Long-lasting facilitation of excitatory postsynaptic potentials in the rat hippocampus by acetylcholine. The Journal of Physiology. 1990 8; 427:381–393. https://doi.org/10.1113/jphysiol.1990.sp018177, doi: 10.1113/jphysiol.1990.sp018177.

McNaughton N, Ruan M, Woodnorth MA. Restoring theta-like rythmicity in rats restores initial learning in the Morris water maze. Hippocampus. 2006 12; 16:1102–1110. https://doi.org/10.1002/hipo.20235, doi: 10.1002/hipo.20235.

Müller C, Remy S. Septo–hippocampal interaction. Cell and Tissue Research. 2018 9; 373:565–575. https://dx.doi.org/10.1007%2Fs00441-017-2745-2, doi: 10.1007/s00441-017-2745-2.

Nachstedt T, Tetzlaff C. Working Memory Requires a Combination of Transient and Attractor-Dominated Dynamics to Process Unreliably Timed Inputs. Scientific Reports. 2017 12; 7:1–14. https://doi.org/10.1038/s41598-017-02471-z, doi: 10.1038/s41598-017-02471-z.

Navaroli VL, Zhao Y, Boguszewski P, Brown TH. Muscarinic receptor activation enables persistent firing in pyramidal neurons from superficial layers of dorsal perirhinal cortex. Hippocampus. 2012 6; 22:1392–1404. http://doi.wiley.com/10.1002/hipo.20975, doi: 10.1002/hipo.20975.

O'Malley JJ, Seibt F, Chin J, Beierlein M. TRPM4 Conductances in Thalamic Reticular Nucleus Neurons Generate Persistent Firing during Slow Oscillations. Journal of Neuroscience. 2020 6; 40:4813–4823. https://doi.org/10.1523/JNEUROSCI.0324-20.2020, doi: 10.1523/JNEUROSCI.0324-20.2020.

Pace RW, Mackay DD, Feldman JL, Negro CAD. Inspiratory bursts in the preBötzinger complex depend on a calcium-activated non-specific cation current linked to glutamate receptors in neonatal mice. Journal of Physiology. 2007 7; 582:113–125. https://dx.doi.org/10.1113%2Fjphysiol.2007.133660, doi: 10.1113/jphysiol.2007.133660.

Pastalkova E, Itskov V, Amarasingham A, Buzsáki G. Internally generated cell assembly sequences in the rat hippocampus. Science. 2008 9; 321:1322–1327. https://science.sciencemag.org/content/321/5894/1322, doi: 10.1126/science.1159775.

Pressler RT, Strowbridge BW. Blanes cells mediate persistent feedforward inhibition onto granule cells in the olfactory bulb. Neuron. 2006 3; 49:889–904. https://doi.org/10.1016/j.neuron.2006.02.019, doi: 10.1016/j.neuron.2006.02.019.

Rahman J, Berger T. Persistent activity in layer 5 pyramidal neurons following cholinergic activation of mouse primary cortices. European Journal of Neuroscience. 2011 7; 34:22–30. http://doi.wiley.com/10.1111/j.1460-9568.2011.07736.x, doi: 10.1111/j.1460-9568.2011.07736.x.

Reboreda A, Jiménez-Díaz L, Navarro-López JD. TRP channels and neural persistent activity. In: *Advances in Experimental Medicine and Biology*, vol. 704 Springer New York LLC; 2011. p. 595–613. https://doi.org/10.1007/978-94-007-0265-3_32, doi: 10.1007/978-94-007-0265-3_32.

Robinson J, Manseau F, Ducharme G, Amilhon B, Vigneault E, Mestikawy SE, Williams S. Optogenetic Activation of Septal Glutamatergic Neurons Drive Hippocampal Theta Rhythms. Journal of Neuroscience. 2016; 36:3016–3023. https://doi.org/10.1523/JNEUROSCI.2141-15.2016, doi: 10.1523/jneurosci.2141-15.2016.

Roland JJ, Stewart AL, Janke KL, Gielow MR, Kostek JA, Savage LM, Servatius RJ, Pang KCH. Medial septum-diagonal band of Broca (MSDB) GABAergic regulation of hippocampal acetylcholine efflux is dependent on cognitive demands. Journal of Neuroscience. 2014 1; 34:506–514. https://doi.org/10.1523/JNEUROSCI.2352-13.2014, doi: 10.1523/JNEUROSCI.2352-13.2014.

Rubin JE, Hayes JA, Mendenhall JL, Negro CAD. Calcium-activated nonspecific cation current and synaptic depression promote network-dependent burst oscillations. Proceedings of the National Academy of Sciences of the United States of America. 2009 2; 106:2939–2944. https://doi.org/10.1073/pnas.0808776106, doi: 10.1073/pnas.0808776106.

Schluppeck D, Curtis CE, Glimcher PW, Heeger DJ. Sustained Activity in Topographic Areas of Human Posterior Parietal Cortex during Memory-Guided Saccades. Journal of Neuroscience. 2006 5; 26:5098–5108. https://doi.org/10.1523/JNEUROSCI.5330-05.2006, doi: 10.1523/JNEUROSCI.5330-05.2006.

Seo H, Barraclough DJ, Lee D. Dynamic Signals Related to Choices and Outcomes in the Dorsolateral Prefrontal Cortex. Cerebral Cortex. 2007 9; 17:i110–i117. https://doi.org/10.1093/cercor/bhm064, doi: 10.1093/cercor/bhm064.

Seo H, Barraclough DJ, Lee D. Lateral intraparietal cortex and reinforcement learning during a mixed-strategy game. Journal of Neuroscience. 2009 6; 29:7278–7279. https://doi.org/10.1523/JNEUROSCI.1479-09.2009, doi: 10.1523/JNEUROSCI.1479-09.2009.

Shirvalkar PR, Rapp PR, Shapiro ML. Bidirectional changes to hippocampal theta-gamma comodulation predict memory for recent spatial episodes. Proceedings of the National Academy of Sciences of the United States of America. 2010 4; 107:7054–7059. https://doi.org/10.1073/pnas.0911184107, doi: 10.1073/pnas.0911184107.

Sosulina L, Mittag M, Geis HR, Hoffmann K, Klyubin I, Qi Y, Steffen J, Friedrichs D, Henneberg N, Fuhrmann F, Justus D, Keppler K, Cuello AC, Rowan MJ, Fuhrmann M, Remy S. Hippocampal hyperactivity in a rat model of Alzheimer's disease. Journal of Neurochemistry. 2021 Mar; https://doi.org/10.1111/jnc.15323, doi: 10.1111/jnc.15323.

Srimal R, Curtis CE. Persistent neural activity during the maintenance of spatial position in working memory. NeuroImage. 2008 1; 39:455–468. https://doi.org/10.1016/j.neuroimage.2007.08.040, doi: 10.1016/j.neuroimage.2007.08.040.

Supèr H, Spekreijse H, Lamme VAF. A neural correlate of working memory in the monkey primary visual cortex. Science. 2001 7; 293:120–124. https://doi.org/10.1126/science.1060496, doi: 10.1126/science.1060496.

Tahvildari B, Alonso AA, Bourque CW. Ionic Basis of <scp>on</scp> and <scp>off</scp> Persistent Activity in Layer III Lateral Entorhinal Cortical Principal Neurons. Journal of Neurophysiology. 2008 4; 99:2006–2011. https://doi.org/10.1152/jn.00911.2007, doi: 10.1152/jn.00911.2007.

Teitelbaum H, Lee JF, Johannessen JN. Behaviorally evoked hippocampal theta waves: A cholinergic response. Science. 1975 6; 188:1114–1116. https://doi.org/10.1126/science.175440, doi: 10.1126/science.175440.

Tian J, Thakur DP, Lu Y, Zhu Y, Freichel M, Flockerzi V, Zhu MX. Dual depolarization responses generated within the same lateral septal neurons by TRPC4-containing channels. Pflugers Archiv European Journal of Physiology. 2014; 466:1301–1316. https://doi.org/10.1007/s00424-013-1362-5, doi: 10.1007/s00424-013-1362-5.

Todd JJ, Marois R. Capacity limit of visual short-term memory in human posterior parietal cortex. Nature. 2004 4; 428:751–754. https://doi.org/10.1038/nature02466, doi: 10.1038/nature02466.

Toth K, Borhegyi Z, Freund TF. Postsynaptic targets of GABAergic hippocampal neurons in the medial septum-diagonal band of Broca complex. Journal of Neuroscience. 1993 9; 13:3712–3724. https://doi.org/10.1523/JNEUROSCI.13-09-03712.1993, doi: 10.1523/jneurosci.13-09-03712.1993.

Turnbull J, Jiang F, Racine R. Hippocampal Stimulation of Fornical-lesioned Rats Improves Working Memory. Canadian Journal of Neurological Sciences / Journal Canadien des Sciences Neurologiques. 1994; 21:100–103. https://doi.org/10.1017/S0317167100049003, doi: 10.1017/S0317167100049003.

Vanderwolf CH. Hippocampal electrical activity and voluntary movement in the rat. Electroencephalography and Clinical Neurophysiology. 1969 4; 26:407–418. https://doi.org/10.1016/0013-4694(69)90092-3, doi: 10.1016/0013-4694(69)90092-3.

Vega-Flores G, Rubio SE, Jurado-Parras MT, Gomez-Climent MA, Hampe CS, Manto M, Soriano E, Pascual M, Gruart A, Delgado-Garcia JM. The GABAergic Septohippocampal Pathway Is Directly Involved in Internal Processes Related to Operant Reward Learning. Cerebral Cortex. 2013 Mar; 24(8):2093–2107. https://doi.org/10.1093/cercor/bht060, doi: 10.1093/cercor/bht060.

Wang Y, Romani S, Lustig B, Leonardo A, Pastalkova E. Theta sequences are essential for internally generated hippocampal firing fields. Nature Neuroscience. 2015 2; 18:282–288. https://doi.org/10.1038/nn.3904, doi: 10.1038/nn.3904.

Whishaw IQ, Vanderwolf CH. Hippocampal EEG and behavior: Change in amplitude and frequency of RSA (Theta rhythm) associated with spontaneous and learned movement patterns in rats and cats. Behavioral Biology. 1973 4; 8:461–484. https://doi.org/10.1016/S0091-6773(73)80041-0, doi: 10.1016/S0091-6773(73)80041-0.

Winson J. Loss of hippocampal theta rhythm results in spatial memory deficit in the rat. Science. 1978 7; 201:160–163. https://doi.org/10.1126/science.663646, doi: 10.1126/science.663646.

Yan HD, Villalobos C, Andrade R. TRPC channels mediate a muscarinic receptor-induced afterdepolarization in cerebral cortex. Journal of Neuroscience. 2009 8; 29:10038–10046. https://dx.doi.org/10.1523%2FJNEUROSCI.1042-09.2009, doi: 10.1523/JNEUROSCI.1042-09.2009.

Yoshida M, Hasselmo ME. Persistent firing supported by an intrinsic cellular mechanism in a component of the head direction system. Journal of Neuroscience. 2009 4; 29:4945–4952. https://doi.org/10.1523/JNEUROSCI.5154-08.2009, doi: 10.1523/JNEUROSCI.5154-08.2009.

Zhang GW, Shen L, Zhong W, Xiong Y, Zhang LI, Tao HW. Transforming Sensory Cues into Aversive Emotion via Septal-Habenular Pathway. Neuron. 2018 9; 99:1016–1028.e5. https://doi.org/10.1016/j.neuron.2018.07.023, doi: 10.1016/J.NEURON.2018.07.023.

Zhang Z, Reboreda A, Alonso A, Barker PA, Séguéla P. TRPC channels underlie cholinergic plateau potentials and persistent activity in entorhinal cortex. Hippocampus. 2011 4; 21:386–397. http://doi.wiley.com/10.1002/hipo.20755, doi: 10.1002/hipo.20755.

Zhou YD, Fuster JM. Mnemonic neuronal activity in somatosensory cortex. Proceedings of the National Academy of Sciences of the United States of America. 1996 9; 93:10533–10537. https://doi.org/10.1073/pnas.93.19.10533, doi: 10.1073/pnas.93.19.10533.

Zylberberg J, Strowbridge BW. Mechanisms of Persistent Activity in Cortical Circuits: Possible Neural Substrates for Working Memory. Annual Review of Neuroscience. 2017 7; 40:603–627. https://doi.org/10.1146/annurev-neuro-070815-014006, doi: 10.1146/annurev-neuro-070815-014006.